For publication in: Insect Biochemistry and Molecular Biology

Running title: SRS1 and SRS6 of CYP6AE determine esfenvalerate metabolism

Roles of the variable P450 substrate recognition sites SRS1 and SRS6 in esfenvalerate metabolism by CYP6AE subfamily enzymes in *Helicoverpa armigera*

Yu Shi[a], Andrias O. O´Reilly[b], Shuo Sun[a], Qiong Qu[a], Yihua Yang[a], Yidong Wu[a]*

[a] College of Plant Protection, Nanjing Agricultural University, Nanjing 210095, China

[b] School of Biological & Environmental Sciences, Liverpool John Moores University, Liverpool, UK

*Corresponding author. College of Plant Protection, Nanjing Agricultural University, Nanjing 210095, China.

E-mail addresses:

yushi@njau.edu.cn (Y. Shi)

a.o.oreilly@ljmu.ac.uk (A. O. O´Reilly)

2018102096@njau.edu.cn (S. Sun)

2018102095@njau.edu.cn (Q. Qu)

yhyang@njau.edu.cn (Y. Yang)

wyd@njau.edu.cn (Y. Wu)

Abstract

The cotton bollworm P450s of the clustered CYP6AE subfamily share high sequence identities but differ dramatically in their capacity to metabolize xenobiotics, especially esfenvalerate. Among them, CYP6AE17 has the highest sequence identity with CYP6AE18 but shows ~7-fold higher metabolic efficiency. CYP6AE11 is most active towards esfenvalerate but CYP6AE20 is inactive even though the enzymes share 54.8% sequence identity. Sequence analysis revealed the SRS1 (Substrate Recognition Site) and SRS6 between CYP6AE17 and CYP6AE18, and SRS1 between CYP6AE11 and CYP6AE20 are the most variable among all six SRSs. In order to identify the key factors that underlie the observed catalytic difference, we exchanged these SRS sequences between two pairs of P450s and studied the activity of the resulting hybrid mutants or chimeras. *In vitro* metabolism showed that the CYP6AE17/18 chimeras had 2- and 10-fold decreased activities and the CYP6AE18/17 chimeras had 6- and 10-fold increased activities to esfenvalerate. Meanwhile, after exchanging SRS1 with each other, the CYP6AE11/20 chimera folded incorrectly but the CYP6AE20/11 chimera gained moderate activity to esfenvalerate. Molecular modeling showed that amino acids variants within SRS1 or SRS6 change the shape and chemical environment of the active sites, which may affect the ligand-binding interactions. These results indicate that the protein structure variation resulting from the sequence diversity of SRSs promotes the evolution of insect chemical defense and contributes to the development of insect resistance to pesticides.

Key words: *Helicoverpa armigera*; Cytochrome P450; SRS exchange; Esfenvalerate; Metabolism; Molecular modeling

1. Introduction

The cotton bollworm, *Helicoverpa armigera* (Hübner), is a global generalist pest that is distributed throughout Europe, Africa, Asia, and South America on over 300 different plant hosts (Tay et al., 2013). Broad host range and wide distribution of this pest lead to increased exposure to different kinds of environmental toxins and to a greater capacity to cope with variable environments (Dermauw et al., 2018). To date, under high selection pressure of pesticides, resistance cases to most insecticide classes and Bt toxins have been reported for this insect (www.pesticideresistance.org). Cytochrome P450-based detoxification was confirmed as one of the most crucial resistance mechanisms within most geographical populations of *H. armigera* (Joußen et al., 2012; Oakeshott et al., 2013; Rasool et al., 2014; Yang et al., 2004, 2005, 2006).

Cytochrome P450 monooxygenases (P450s) are an important superfamily of hemoproteins, found in almost all organisms, which participate in the biosynthesis and metabolism of endogenous compounds and the detoxification of xenobiotics (Feyereisen, 2012). P450s play a crucial role in the survival of insects. In addition to being intermediates in basal physiological metabolism, most insect P450s are involved in the detoxification of insecticides and phytochemicals. The catalytic capability and efficiency of P450s are determined by structure, especially the amino acids that determine the shape and size of the active site. Analyses of available mammalian and microbial P450 structures revealed that the overall three-dimensional structures of P450s are conserved despite an often low amino acid sequence identity (Feyereisen, 2012; Guengerich et al., 2016). Comparisons of primary sequences have suggested that six substrate recognition sites (SRSs) with highly variable sequences account for the diverse range of the substrate specificities of P450s (Gotoh, 1992). Extensive site-directed mutagenesis studies have shown that SRSs constitute several important domains within the tertiary structure of P450 proteins and contribute to function (Chen et al., 2002; Paine et al., 2003; Pan et al., 2004). The P450 catalytic site is mainly determined by SRS1, SRS4, SRS5 and SRS6 and the substrate access channel is shaped mainly by SRS2 and SRS3 (Schuler et al., 2013). While it is clear that the SRSs play significant roles in defining enzyme activity and substrate ranges in various bacterial, mammalian and insect P450s, our understanding of relationships between SRS sequences and enzyme properties remains poor. For example, many closely-related P450s

display differences in substrate metabolism whereas phylogenetically distinct P450s may metabolize similar substrates (Rupasinghe et al., 2007; Wang et al., 2018). Nevertheless, the variations of P450 activities or substrate profiles mediated by SRS can reveal the evolution and divergence of P450 orthologs or paralogs (Dueholm et al., 2015; Li et al., 2003; Wen et al., 2006).

A typical "bloom" of CYP genes (Feyereisen, 2011), the CYP6AE subfamily has expanded in several lepidopteran insects (Calla et al., 2017; Shi et al., 2018). It is one of the principal P450 subfamilies responsible for the ability of *H. armigera* larvae to detoxify xenobiotics (Krempl et al., 2016; Shi et al., 2018; Wang et al., 2018). Many CYP6AE are constitutively overexpressed in pyrethroid resistant *H. armigera* strains (Barale et al., 2010; Rasool et al., 2014) and over half the members of the CYP6AE subfamily in *H. armigera* are transcriptionally sensitive to over ten kinds of plant allelochemicals and synthetic compounds (Celorio-Mancera et al., 2011; Krempl et al., 2016; Mao et al., 2007; Tao et al., 2012; Zhang et al., 2016; Zhou et al., 2010; Pearce et al., 2017). Complete *in vivo* and *in vitro* tests provided direct evidence that CYP6AEs are involved in the detoxification of xanthotoxin, 2-tridecanone, esfenvalerate, indoxacarb, imidacloprid and aldrin (Shi et al., 2018; Wang et al., 2018), thus showing that they play a crucial role in the chemical defense of *H. armigera*. Ten CYP6AE subfamily members share high amino acid sequence identities (up to 91.8%) but exhibit great variation in metabolic activities. In particular, *in vitro* metabolism of esfenvalerate revealed a greater than 40-fold efficiency difference between CYP6AE11/14 and CYP6AE19/20 clades which share ~55% sequence similarity; CYP6AE20 even lacked metabolic capacity toward this pyrethroid. In addition, the *V*max of CYP6AE17 was 15-fold higher than CYP6AE18 resulting in a ~7-fold efficiency difference despite the fact that they share 91.8% sequence identity (Shi et al., 2018). We hypothesize that sequence variants within the SRS regions are major determinants of the large metabolic differences observed in this CYP6AE subfamily.

In this study, we analyzed the sequences of two distinctive CYP6AE P450 pairs: CYP6AE11-CYP6AE20 and CYP6AE17-CYP6AE18. Six CYP6AE sequence hybrids of chimeras were generated by exchanging the SRS1 and SRS6 sections of the parent sequences, as these were shown to be the most variable SRS regions. The metabolic activities of wild-type and mutant CYP6AE enzymes were determined using esfenvalerate as the substrate. Molecular

modelling was also performed to identify amino acids that may contribute to ligand-binding interactions.

2. Materials and methods

2.1 *Reagents and Chemicals*

Enzymes for DNA fragment cloning (Q5 High-Fidelity DNA Polymerase), digestion (restriction enzymes) and linkage (T4 ligase) were supplied by New England Biolabs Company (Ipswich, MA). Esfenvalerate was purchased from Dr. Ehrentsorfer GmbH (Augsburg, Germany). HPLC solvents were purchased from Fisher Scientific (Pittsburgh, Pennsylvania).

2.2 *Construction and functional expression of P450 hybrid mutants*

The wild-type *CYP6AE11*, *CYP6AE20*, *CYP6AE17* and *CYP6AE18* were previously subcloned into pFastBacHTA (Shi et al., 2018). The mutants were constructed by fusion PCR. SRS1 or SRS6 and their flanking sequences with overlap sequence were cloned separately. Two flanking sequences and target SRS sequence were linked by a second round of PCR with full-length primers (Fig. S1). The primers used for cloning are shown in Table S1. All mutants were cloned into pFastBacHTA vector (Invitrogen). The baculovirus plasmid was produced and transfected into Sf9 cells according to the Bac-to-Bac baculovirus expression system (Invitrogen) as described (Shi et al., 2018). The P450 mutants and non-insertion control were coexpressed with *H. armigera* cytochrome P450 reductase (HaCPR) in High Five cells (Invitrogen); the multiplicity of infection (MOI) of P450 and HaCPR was 2 and 0.2, respectively. Microsomes were purified by differential centrifugation. The recombinant P450 was identified by Western blot with 6×His tag antibody (Abcam, Cambridge, UK) and quantified by reduced CO-difference spectra assay (Omura et al., 1964).

2.3 *Esfenvalerate metabolism and UPLC-MS/MS analysis*

The metabolism of esfenvalerate was performed with 0.1mg microsomes containing recombinant P450 or non-insertion control. The *in vitro* metabolism system was incubated in 200 µl 0.1 M potassium phosphate buffer (pH 7.4) in 1.5 ml Eppendorf tube with an NADPH-regenerating system (1.3 mM $NADP^+$, 3.3 mM glucose-6-phosphate, 3.3 mM $MgCl_2$ and 0.4

U/mL glucose-6-phosphate dehydrogenase) and 1μl esfenvalerate (5 μM, freshly dissolved in acetonitrile). Reactions were pre-warmed in 30 ºC for 5 min and started after adding insecticide. Samples were incubated at 30 ºC, 1,200 rpm for 1h and reactions were stopped by adding 200 μl acetonitrile and incubating for a further 20 min. Samples were centrifuged at 18,000×g for 15min before being transferred to HPLC vials and analyzed immediately by tandem mass spectrometry as described (Shi et al., 2018). Samples without NADPH were performed at the same time. The final metabolic activity was corrected by subtracting the background (non-insertion control) and expressed as pmol 4'-hydroxy-metabolite per minute per mg protein. For the kinetic assay, 10 pmol P450 was used in each sample and suitable ranges of substrate concentrations for each P450 were performed after several pre-tests.

2.4 Homology modelling and automated ligand docking

Chain A of the human cytochrome P450 CYP3A5 X-ray crystal structure (PDB code 5VEU) (Hsu et al., 2018) provided the template for homology modelling of the CYP6AE11, CYP6AE20, CYP6AE17 and CYP6AE18 enzymes. A multiple sequence alignment was performed using Clustal Omega (Sievers et al., 2011). Each homology model was generated using MODELLER (Eswar et al., 2006) to produce 50 starting models. The internal scoring function of MODELLER was used to select 10 models that were visually inspected and submitted to the VADAR webserver (Willard et al., 2003) for assessment of stereochemical soundness, with the best model selected based on these structural evaluations.

A structure for esfenvalerate was generated *ab initio* using MarvinSketch (version 5.9.1) of the ChemAxon suite (http://www.chemaxon.com). AutoDockTools (version 1.5.4) (Molecular Graphics Laboratory, Scripps Research Institute, La Jolla, CA, USA) was used to define rotatable bonds in esfenvalerate and merge the non-polar hydrogens. Automated ligand docking studies of esfenvalerate with CYP6AE homology models were performed using Auto-Dock Vina (version 1.1.2) (Trott et al., 2010) with a grid of 40 × 40 × 40 points (1 Å spacing) centred on the enzyme's central cavity. Docking predictions were screened by interaction energy and by selecting poses where the esfenvalerate phenoxyphenyl group was <4.5 Å distance from the enzyme heme group.

The volume of each enzyme's active site cavity was plotted using Caver3 (Chovancova et

al., 2012) with a probe radius of 1.5 Å, shell radius of 3 Å and a shell depth of 4 Å. Figures were produced using PyMOL (DeLano Scientific, San Carlos, CA, USA).

3 Results

3.1 Amino acid sequence analysis of four CYP6AE P450 genes

The sequences of *CYP6AE11*, *CYP6AE20*, *CYP6AE17* and *CYP6AE18* are shown in Fig. 1. CYP6AE11 and CYP6AE20 have low sequence identities in SRS1, SRS3 and SRS6, and SRS1 shows the lowest identity between the two genes (fifteen substitutions with eleven nonsynonymous substitutions) (Table S2). CYP6AE17 shares high sequence identity with CYP6AE18 with the exception of SRS1 (five nonsynonymous substitutions) and SRS6 (four nonsynonymous substitutions). In order to explore the significance of these diverse SRSs in the metabolism of esfenvalerate, we exchanged SRS1 between CYP6AE11 and CYP6AE20 to create CYP6AE11-20SRS1 and CYP6AE20-11SRS1 chimeric enzymes. In addition, SRS1 and SRS6 were exchanged between CYP6AE17 and CYP6AE18 to create CYP6AE17-18SRS1, CYP6AE17-18SRS6, CYP6AE18-17SRS1 and CYP6AE18-17SRS6 (Fig. 2).

3.2 Functional expression of six mutants in High Five cell line

The recombinant P450s and HaCPR in purified microsomes were identified by Western blot (Fig. 3A). The six chimeras migrated between 50-60kDa and HaCPR located near 75kDa as predicted. Reduced CO-difference spectrum of each individually expressed protein revealed that all generated CO-spectrum maxima near 450nm except CYP6AE11-20SRS1. A significantly high concentration of P420 could be detected in recombinant CYP6AE11-20SRS1 but no peak could be found near 450nm under a variety of expression and detection conditions (Fig. 3B).

3.3 Metabolism of esfenvalerate

The results of *in vitro* metabolism revealed that all six P450 mutants could metabolize esfenvalerate because the formation of 4’-hydroxy-esfenvalerate in each sample was significantly higher than the non-insertion control incubated under the same conditions (Fig. 4).

The 4’-hydroxy-esfenvalerate formation rates of each recombinant mutant in response to

esfenvalerate concentration revealed Michaelis-Menten kinetics (Fig. S2). The metabolic capabilities of six mutants to esfenvalerate varied considerably (Table 1). Compared with wild-type CYP6AE P450s, the chimera CYP6AE20-11SRS1 (CYP6AE20 with the SRS1 from CYP6AE11) gained a moderate ability (*V*max/*K*m) to metabolize esfenvalerate. CYP6AE11-20SRS1 showed similar affinity (*K*m) to esfenvalerate as wild type. As no peak near 450 nm could be detected in the CO-difference spectrum of CYP6AE11-20SRS1, the concentration of recombinant P450 in the microsomal protein could not be measured accurately and so the final enzyme activity was corrected by mg protein. Meanwhile, the substitution of SRS1 had a great impact on CYP6AE17 as the *V*max of CYP6AE17-18SRS1 decreased ten-fold and ultimately resulted in a ~13-fold decrease in metabolic efficiency (*V*max/*K*m). In contrast, the exchange of SRS6 produced a lesser effect on CYP6AE17 with a ~2-fold decrease in both substrate affinity and metabolic efficiency for CYP6AE17-18SRS6 compared with wild-type CYP6AE17. On the other hand, the *V*max of CYP6AE18 increased 15-fold after the exchange of SRS1 from CYP6AE17 and, while the affinity decreased slightly, there was an overall ~6-fold increase in metabolic efficiency. With regards the SRS6 region, the *V*max of CYP6AE18 increased 7-fold when the 5 amino acids were substituted to their CYP6AE17 equivalents and there was a slight increase in affinity to esfenvalerate, which ultimately increased the efficiency (*V*max/*K*m) by an order of magnitude.

3.4 Active site cavities and esfenvalerate binding interactions in CYP6AE models

Homology models of the wild-type CYP6AE11, CYP6AE17, CYP6AE18 and CYP6AE20 enzymes were generated based on the structure of the human cytochrome P450 CYP3A5 (Hsu et al., 2018). This template was chosen due to its high-resolution (2.91 Å) and its 28-29% sequence identity with the four *H. armigera* enzymes (Fig. S3). Analysis of the homology models identified a number of SRS1 and SRS6 residues that line the active site cavity and may therefore be positioned to make ligand-binding interactions (Fig. 5A).

Fig. 5B shows the variation in the volumes of the active site cavities, with CYP6AE17 and CYP6AE18 having more voluminous cavities than CYP6AE11 and CYP6AE20. In particular, the aromatic side chain of SRS6 F496 (residues in all models are numbered according to the CYP6AE11 sequence to enable comparisons) projects into the CYP6AE11 and CYP6AE20

cavities to constrict the active site. There is an additional aromatic side chain (F121) in the CYP6AE20 enzyme that projects into the cavity whereas this 121 position on SRS1 is occupied by the smaller side-chain alanine or serine in CYP6AE11, CYP6AE17 and CYP6AE18. Accordingly, a docking prediction of esfenvalerate and with an estimated -9.5 kcal/mol binding affinity shows the ligand folded in the tightly confined space of the CYP6AE20 cavity. In contrast esfenvalerate adopts a more elongated pose when occupying the active sites of CYP6AE11 (-9.1 kcal/mol), CYP6AE17 (-9.2 kcal/mol) and CYP6AE18 (-8.4 kcal/mol) (Fig. 5B).

The SRS1 109 residue is phenylalanine in CYP6AE17 but tyrosine in CYP6AE18 whereas the SRS6 496 residue is threonine in CYP6AE17 but isoleucine in CYP6AE18. The hydroxyl group of Y109 projects into the CYP6AE18 cavity as does the I496 side chain therefore presenting different chemical groups to the active site. Similarly, the SRS1 112 position is occupied by the small side-chain serine residue in CYP6AE20 but by a positively-charged amino acid in CYP6AE11, CYP6AE17 and CYP6AE18. The CYP6AE17 R112 side chain is 4.8 Å from the esfenvalerate cyano-group nitrogen, the CYP6AE18 R112 side chain is 3.2 Å from the ligand's carbonyl oxygen and the α-amino of the CYP6AE11 K112 side chain is 5.55 Å from the ligand cyano nitrogen. As discussed below, the amino acid variants at these identified positions may underlie the different activities of the P450s towards esfenvalerate.

4 Discussion

In this study, we demonstrate using chimeric enzymes generated by fragment substitution that the SRS1 and SRS6 regions have a major impact on protein folding and metabolic capability of the CYP6AE enzymes. The metabolic efficiencies of mutants from CYP6AE17 and CYP6AE18 changed significantly after exchange of their SRS1 or SRS6 sections. Most notable is the activity of the CYP6AE20-11SRS1 construct given the lack of metabolic activity of the wild-type CYP6AE20 towards esfenvalerate.

To date, multiple site-directed mutagenesis studies have demonstrated that amino acids in SRSs affect the protein folding and substrate range of cytochrome P450s. Among the six SRS regions, the SRS1 in a loop region, close to the active site heme, has proven to be the most important SRS that affects multiple properties of P450s (Domanski et al., 2001; Graham-

Lorence et al., 1996; Schuler et al., 2013). In the CYP6B subfamily, several conserved amino acids in SRS1 and variable positions in SRS6 are proposed to form an aromatic-aromatic resonant network that maintains the hydrophobic catalytic pocket and determines substrate turnover/specificity (Baudry et al., 2003; Chen et al., 2002). Two variable amino acids, Ile115 and A113, in the SRS1 of CYP6B subfamily proteins, form a hydrogen bond network that controls the spin state of the heme and effects the catalytic activity and substrate range (Pan et al., 2004). In *H. armigera*, there is an example of a natural chimera, CYP337B3, a gene conversion product (from unequal crossing-over) which consists of the partial N-terminal sequence with SRS1 from its paralog CYP337B2 and the C-terminal part of the other paralog CYP337B1. This new gene product can metabolize fenvalerate and cypermethrin while its originator paralogs cannot (Joußen et al., 2012; Rasool et al., 2014). In our study, it was also demonstrated that SRS1 and SRS6 regions affected the fenvalerate metabolism efficiency of *H. armigera* CYP6AE P450s. In addition, it has been reported that the formation of CO-difference maxima at 420nm might result from conformational changes that restricts substrate access and binding in the catalytic site (Martinis et al., 1996). In our study, CYP6AE11-20SRS1 formed no peak at 450nm but significant activity to esfenvalerate could nonetheless be detected in *in vitro* metabolism. Possibly this protein sample consisted of an abundance of P420 with a concentration of correctly-folded P450 that was too low to be detected by the reduced CO-difference spectrum assay. Alternatively, the conformational change induced by substrate binding might restore a normal heme-thiolate environment.

There are a number of mechanisms by which a change in a P450 sequence can result in altered function (Schuler et al., 2013). One mechanism is that the access channel gets reshaped, which subsequently affects substrate entry. Analysis of mosquito P450 enzyme models suggests that a lack of capability to metabolism pyrethroids is associated with a SRS1 arginine (R114) that projects into the access channel to restrict substrate ingress (Lertkiatmongkol et al., 2011). The equivalent SRS1 residue – D111, H111 or G111 (numbered according to the CYP6AE11 sequence) – in the four *H. armigera* enzymes of this study have comparatively smaller side chains than arginine and therefore may not present comparable steric hindrance to substrate entry. Instead a change to the shape, flexibility or hydrophobicity of the active site may account for the effect of the SRS1 or SRS6 exchange. For example, an aromatic residue F496 on the

SRS6 of CYP6AE11 and CYP6AE20 (but not present in CYP6AE17 or CYP6AE18) occupies space near the heme group and may obstruct approach of the substrate. It was proposed that a phenylalanine in the equivalent position in CYP9Q2 enzyme (F491) was a binding contact for tau-fluvalinate (Mao et al., 2007). Future mutagenesis studies can reveal the degree to which size or the presence of an aromatic ring at this position impacts enzyme reactivity. Similarly, we have identified other active site residues that merit investigation of physicochemical properties including the SRS1 residue at position 112. This residue is positively-charged in CYP6AE11, CYP6AE17 and CYP6AE18 and may form electrostatic interactions with electronegative groups on the pyrethroid and consequently help orientate the substrate for reaction. In CYP6AE20 this position is occupied by a small polar residue (S112) and this may be a contributing factor for the inactivity of CYP6AE20 towards esfenvalerate in contrast to the metabolic capability of the CYP6AE20-11SRS1 chimera.

The multiple duplications of P450 genes leading to CYP blooms (Feyereisen, 2011) can result in versatile and enhanced detoxification capacities. The accumulated variation within SRSs of duplicated alleles (Zimmer et al., 2018) or paralogs (Mao et al., 2009, 2011; Shi et al., 2018; Li et al., 2003; Manjon et al., 2018; Troczka et al., 2019) is associated with novel functions or with higher detoxification capability to certain compounds. As most CYP6AE P450s in *H. armigera* can metabolize esfenvalerate with different efficiencies and are easily induced by xenobiotics (Shi et al., 2018; Wang et al., 2018), it is possible that certain field strains could gain resistance to fenvalerate rapidly by selection of CYP6AE variants that are easily induced, constitutively overexpressed or with higher metabolic efficiency, or indeed with a combination of such traits. In this sense, the structure-derived functional divergence among members of a CYP cluster may contribute to the development of insecticide resistance.

In summary, a clustered P450 subfamily such as the CYP6AE, with high sequence identity and known catalytic capacity constitutes a great material to study the structure-based functional diversity and evolution of insect P450s. Our findings not only identified molecular determinants of the dramatic difference in esfenvalerate metabolism between *H. armigera* CYP6AE P450s, but also provide a basis for further research on the functional divergence of this subfamily and other insect P450 subfamilies blooms.

Acknowledgements

This work was supported by the National Natural Science Foundation of China (grant no. 31901887), the Fundamental Research Funds for the Central Universities (grant no. KJQN202010) and the SAFEA of China (grant no. BP0719029). We thank René Feyereisen for his interest and critical reading of the manuscript.

References

Barale, A.B., Héma, O., Martin, T., Suraporn, S., Audant, P., Sezutsu, H., Feyereisen, R., 2010. Multiple P450 genes overexpressed in deltamethrin-resistant strains of *Helicoverpa armigera*. Pest Manag. Sci. 66, 900-909.

Baudry, J., Li, W., Pan, L., Berenbaum, M.R., Schuler, M.A., 2003. Molecular docking of substrates and inhibitors in the catalytic site of CYP6B1, an insect cytochrome P450 monooxygenase. Protein Eng. Des. Sel. 16, 577-587.

Calla, B., Noble, K., Johnson, R.M., Walden, K.K.O., Schuler, M.A., Robertson, H.M., Berenbaum, M.R., 2017. Cytochrome P450 diversification and hostplant utilization patterns in specialist and generalist moths: Birth, death and adaptation. Mol. Ecol. 26, 6021-6035.

Celorio-Mancera, M., Ahn, S.J., Vogel, H., Heckel, D.G., 2011. Transcriptional responses underlying the hormetic and detrimental effects of the plant secondary metabolite gossypol on the generalist herbivore *Helicoverpa armigera*. BMC Genomics 1, 575.

Chen, J.S., Berenbaum, M.R., Schuler, M.A., 2002. Amino acids in SRS1 and SRS6 are critical for furanocoumarin metabolism by CYP6B1v1, a cytochrome P450 monooxygenase. Insect Mol. Biol. 11, 175-186.

Chovancova, E., Pavelka, A., Benes, P., Strnad, O., Brezovsky, J., Kozlikova, B., Gora, A., Sustr, V., Klvana, M., Medek, P., Biedermannova, L., Sochor, J., Damborsky, J., 2012. CAVER 3.0: A tool for the analysis of transport pathways in dynamic protein structures. PLoS Comput. Biol. 8, e1002708.

Dermauw, W., Pym, A., Bass, C., Van Leeuwen, T., Feyereisen, R., 2018. Does host plant adaptation lead to pesticide resistance in generalist herbivores? Curr. Opin. Insect Sci. 26, 25-33.

Domanski, T.L., Halpert, J.R., 2001. Analysis of mammalian cytochrome P450 structure and function by site-directed mutagenesis. Curr. Drug Metab. 2, 117-137.

Dueholm, B.R., Krieger, C., Drew, D., Olry, A., Kamo, T., Taboureau, O., Weitzel, C., Bourgaud, F., Hehn, A., Simonsen, H.T., 2015. Evolution of substrate recognition sites (SRSs) in cytochromes P450 from Apiaceae exemplified by the CYP71AJ subfamily. BMC Evol. Biol. 15, 122.

Eswar, N., Webb, B., Marti-Renom, M.A., Madhusudhan, M.S., Eramian, D., Shen, M.Y.,

Pieper, U., Sali, A., 2006. Comparative protein structure modeling using Modeller. Curr. Protoc. Bioinformatics Chapter 5, unit 5-6.

Feyereisen, R., 2011. Arthropod CYPomes illustrate the tempo and mode in P450 evolution. Biochim. Biophys. Acta 1814: 19-28.

Feyereisen, R., 2012. Insect CYP genes and P450 enzymes, in: Gilbert, L.I.(Ed.), Insect Molecular Biology and Biochemistry. Elsevier B.V., London. 236-316.

Gotoh, O., 1992. Substrate recognition sites in cytochrome P450 family 2 (CYP2) proteins inferred from comparative analyses of amino acid and coding nucleotide sequences. J. Biol. Chem. 267, 83-90.

Graham-Lorence, S., Peterson, J.A., 1996. P450s: Structural similarities and functional differences. Faseb J. 10, 206-214.

Guengerich, F.P., Waterman, M.R., Egli, M., 2016. Recent Structural Insights into Cytochrome P450 Function. Trends Pharmacol. Sci. 37, 625-640.

Hsu, MH., Savas, U., Johnson, E.F., 2018. The X-Ray crystal structure of the human Mono-Oxygenase cytochrome P450 3A5-Ritonavir complex reveals active site differences between P450s 3A4 and 3A5. Mol. Pharmacol. 93, 14-24.

Joußen, N., Agnolet, S., Lorenz, S., Schöene, S.E., Ellinger, R., Schneider, B., Heckel, D.G., 2012. Resistance of Australian *Helicoverpa armigera* to fenvalerate is due to the chimeric P450 enzyme CYP337B3. Proc. Natl. Acad. Sci. U.S.A. 109, 15206-15211.

Krempl, C., Heidel-Fischer, H.M., Jimenez-Aleman, G.H., Reichelt, M., Menezes, R.C., Boland, W., Vogel, H., Heckel, D.G., Joussen, N., 2016. Gossypol toxicity and detoxification in *Helicoverpa armigera* and *Heliothis virescens*. Insect Biochem. Mol. Biol. 78, 69-77.

Lertkiatmongkol, P., Jenwitheesuk, E., Rongnoparut, P., 2011. Homology modeling of mosquito cytochrome P450 enzymes involved in pyrethroid metabolism: Insights into differences in substrate selectivity. BMC Res. Notes 4, 321.

Li, W., Schuler, M.A., Berenbaum, M.R., 2003. Diversification of furanocoumarin-metabolizing cytochrome P450 monooxygenases in two *papilionids*: Specificity and substrate encounter rate. Proc. Natl. Acad. Sci. U.S.A. 100, 14593-14598.

Liu, W., Xie, Y., Ma, J., Luo, X., Nie, P., Zuo, Z., Lahrmann, U., Zhao, Q., Zheng, Y., Zhao, Y., 2015. IBS: An illustrator for the presentation and visualization of biological sequences. Bioinformatics 31, 3359-3361.

Manjon, C., Troczka, B.J., Zaworra, M., Beadle, K., Randall, E., Hertlein, G., Singh, K.S., Zimmer, C.T., Homem, R.A., Lueke, B., Reid, R., Kor, L., Kohler, M., Benting, J., Williamson, M.S., Davies, T.G.E., Field, L.M., Bass, C., Nauen, R., 2018. Unravelling the molecular determinants of bee sensitivity to neonicotinoid insecticides. Curr. Bio. 28, 1137-1143.

Mao, W., Rupasinghe, S.G., Johnson, R.M., Zangerl, A.R., Schuler, M.A., Berenbaum, M.R.,

2009. Quercetin-metabolizing CYP6AS enzymes of the pollinator *Apis mellifera* (Hymenoptera: Apidae). Comp. Biochem. Physiol. B Biochem. and Mol. Bio. 154, 427-434.

Mao, W., Schuler, M.A., Berenbaum, M.R., 2011. CYP9Q-mediated detoxification of acaricides in the honey bee (*Apis mellifera*). Proc. Natl. Acad. Sci. U.S.A. 108, 12657-12662.

Mao, Y., Cai, W., Wang, J., Hong, G., Tao, X., Wang, L., Huang, Y., Chen, X., 2007. Silencing a cotton bollworm P450 monooxygenase gene by plant-mediated RNAi impairs larval tolerance of gossypol. Nat. Biotechnol. 25, 1307-1313.

Martinis, S.A., Blanke, S.R., Hager, L.P., Sligar, S.G., Hoa, G.H., Rux, J.J., Dawson, J.H., 1996. Probing the heme iron coordination structure of pressure-induced cytochrome P420cam. Biochemistry 35, 14530-14536.

Oakeshott, J.G., Farnsworth, C.A., East, P.D., Scott, C., Han, Y., Wu, Y., Russell, R.J., 2013. How many genetic options for evolving insecticide resistance in heliothine and spodopteran pests? Pest Manag. Sci. 69, 889-896.

Omura, T., Sato, R., 1964. The carbon monoxide-binding pigment of liver microsomes. I. Evidence for its hemoprotein nature. J. Biol. Chem. 239, 2370-2378.

Paine, M.J., McLaughlin, L.A., Flanagan, J.U., Kemp, C.A., Sutcliffe, M.J., Roberts, G.C., Wolf, C.R., 2003. Residues glutamate 216 and aspartate 301 are key determinants of substrate specificity and product regioselectivity in cytochrome P450 2D6. J. Biol. Chem. 278, 4021-4027.

Pan, L., Wen, Z., Baudry, J., Berenbaum, M.R., Schuler, M.A., 2004. Identification of variable amino acids in the SRS1 region of CYP6B1 modulating furanocoumarin metabolism. Arch. Biochem. Biophys. 422, 31-41.

Pearce, S.L., Clarke, D.F., East, P.D., Elfekih, S., Gordon, K.H.J., Jermiin, L.S., McGaughran, A., Oakeshott, J.G., Papanikolaou, A., Perera, O.P., Rane, R.V., Richards, S., Tay, W.T., Walsh, T.K., Anderson, A., Anderson, C.J., Asgari, S., Board, P.G., Bretschneider, A., Campbell, P.M., Chertemps, T., Christeller, J.T., Coppin, C.W., Downes, S.J., Duan, G., Farnsworth, C.A., Good, R.T., Han, L.B., Han, Y.C., Hatje, K., Horne, I., Huang, Y.P., Hughes, D.S.T., Jacquin-Joly, E., James, W., Jhangiani, S., Kollmar, M., Kuwar, S.S., Li, S., Liu, N., Maibeche, M.T., Miller, J.R., Montagne, N., Perry, T., Qu, J., Song, S.V., Sutton, G.G., Vogel, H., Walenz, B.P., Xu, W., Zhang, H., Zou, Z., Batterham, P., Edwards, O.R., Feyereisen, R., Gibbs, R.A., Heckel, D.G., McGrath, A., Robin, C., Scherer, S.E., Worley, K.C., Wu, Y.D., 2017. Genomic innovations, transcriptional plasticity and gene loss underlying the evolution and divergence of two highly polyphagous and invasive helicoverpa pest species. BMC Biol. 15, 63.

Rasool, A., Joußen, N., Lorenz, S., Ellinger, R., Schneider, B., Khan, S.A., Ashfaq, M., Heckel, D.G., 2014. An independent occurrence of the chimeric P450 enzyme CYP337B3 of *Helicoverpa armigera* confers cypermethrin resistance in Pakistan. Insect Biochem. Mol. Biol. 53, 54-65.

Rupasinghe, S.G., Wen, Z., Chiu, T.L., Schuler, M.A., 2007. *Helicoverpa zea* CYP6B8 and

CYP321A1: Different molecular solutions to the problem of metabolizing plant toxins and insecticides. Protein Eng. Des. Sel. 20, 615-624.

Schuler, M.A., Berenbaum, M.R., 2013. Structure and function of cytochrome P450s in insect adaptation to natural and synthetic toxins: Insights gained from molecular modeling. J. Chem. Ecol. 39, 1232-1245.

Shi, Y., Wang, H., Liu, Z., Wu, S., Yang, Y., Feyereisen, R., Heckel, D.G., Wu, Y., 2018. Phylogenetic and functional characterization of ten P450 genes from the CYP6AE subfamily of *Helicoverpa armigera* involved in xenobiotic metabolism. Insect Biochem. Mol. Biol. 93, 79-91.

Sievers, F., Wilm, A., Dineen, D., Gibson, T.J., Karplus, K., Li, W., Lopez, R., McWilliam, H., Remmert, M., Soding, J., Thompson, J.D., Higgins, D.G., 2011. Fast, scalable generation of high-quality protein multiple sequence alignments using Clustal Omega. Mol. Syst. Biol. 7, 539.

Tao, X., Xue, X., Huang, Y., Chen, X., Mao, Y., 2012. Gossypol-enhanced P450 gene pool contributes to cotton bollworm tolerance to a pyrethroid insecticide. Mol. Ecol. 21, 4371-4385.

Tay, W.T., Soria, M.F., Walsh, T.K., Thomazoni, D., Silvie, P., Behere, G.T., Anderson, C., Downes, S., 2013. A brave new world for an old world pest: *Helicoverpa armigera* (Lepidoptera: Noctuidae) in brazil. PLoS One 8, e80134.

Troczka, B.J., Homem, R.A., Reid, R., Beadle, K., Kohler, M., Zaworra, M., Field, L.M., Williamson, M.S., Nauen, R., Bass, C., Davies, T.G.E., 2019. Identification and functional characterisation of a novel N-cyanoamidine neonicotinoid metabolising cytochrome P450, CYP9Q6, from the buff-tailed bumblebee Bombus terrestris. Insect Biochem. Mol. Biol. 111, 103171.

Trott, O., Olson, A.J., 2010. AutoDock Vina: Improving the speed and accuracy of docking with a new scoring function, efficient optimization, and multithreading. J. Comput. Chem. 31, 455-461.

Wang, H., Shi, Y., Wang, L., Liu, S., Wu, S., Yang, Y., Feyereisen, R., Wu, Y., 2018. CYP6AE gene cluster knockout in *Helicoverpa armigera* reveals role in detoxification of phytochemicals and insecticides. Nat. Commun. 9, 4820.

Wen, Z., Rupasinghe, S., Niu, G., Berenbaum, M.R., Schuler, M.A., 2006. CYP6B1 and CYP6B3 of the black swallowtail (*Papilio polyxenes*): Adaptive evolution through subfunctionalization. Mol. Biol. Evol. 23, 2434-2443.

Willard, L., Ranjan, A., Zhang, H., Monzavi, H., Boyko, R.F., Sykes, B.D., Wishart, D.S., 2003. VADAR: A web server for quantitative evaluation of protein structure quality. Nucleic Acids Res. 31, 3316-3319.

Yang, E., Yang, Y., Wu, S., Wu, Y., 2005. Relative contribution of detoxifying enzymes to pyrethroid resistance in a resistant strain of *Helicoverpa armigera*. J. Appl. Entomol. 129, 521-525.

Yang, Y., Chen, S., Wu, S., Yue, L., Wu, Y., 2006. Constitutive overexpression of multiple cytochrome P450 genes associated with pyrethroid resistance in *Helicoverpa armigera.* J. Econ. Entomol. 99, 1784-1789.

Yang, Y., Wu, Y., Chen, S., Devine, G.J., Denholm, I., 2004. The involvement of microsomal oxidases in pyrethroid resistance in *Helicoverpa armigera* from Asia. Insect Biochem. Mol. Biol. 34, 763-773.

Zhang, L., Lu, Y., Xiang, M., Shang, Q., Gao, X., 2016. The retardant effect of 2-Tridecanone, mediated by Cytochrome P450, on the Development of Cotton bollworm, *Helicoverpa armigera*. BMC Genomics 17, 954.

Zhou, X., Sheng, C., Li, M., Wan, H., Liu, D., 2010. Expression responses of nine cytochrome P450 genes to xenobiotics in the cotton bollworm *Helicoverpa armigera*. Pest. Biochem. Physiol. 97, 209-213.

Zimmer, C.T., Garrood, W.T., Singh, K.S., Randall, E., Lueke, B., Gutbrod, O., Matthiesen, S., Kohler, M., Nauen, R., Davies, T.G.E., Bass, C., 2018. Neofunctionalization of duplicated P450 genes drives the evolution of insecticide resistance in the brown planthopper. Curr. Biol. 28, 268-274.

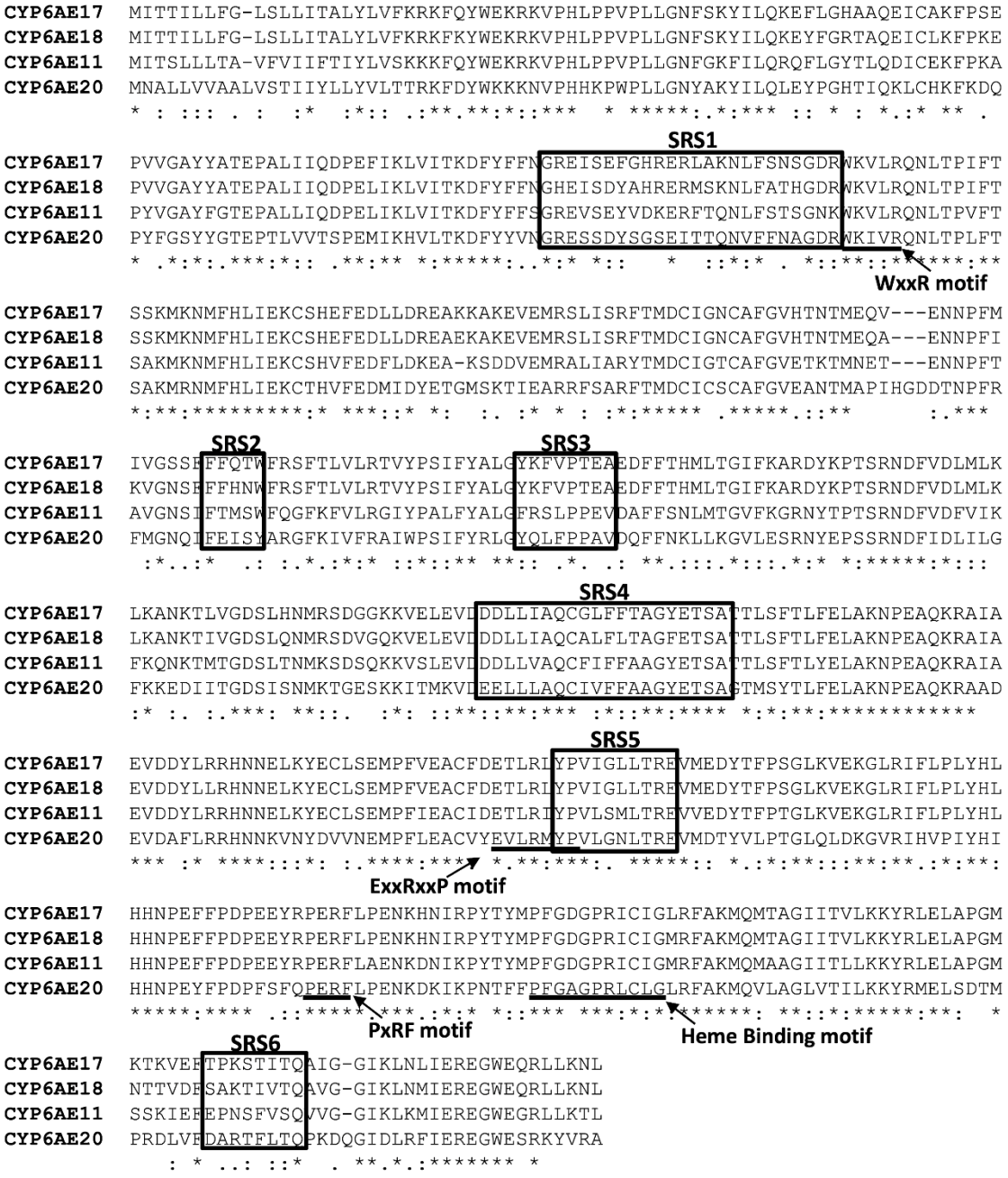

Figure 1. Primary sequences of four CYP6AE proteins. Four conserved motifs: WxxxR motif, ExxRxxP motif, PxRF motif and Heme binding site are underlined. The six SRS regions are enclosed in boxes.

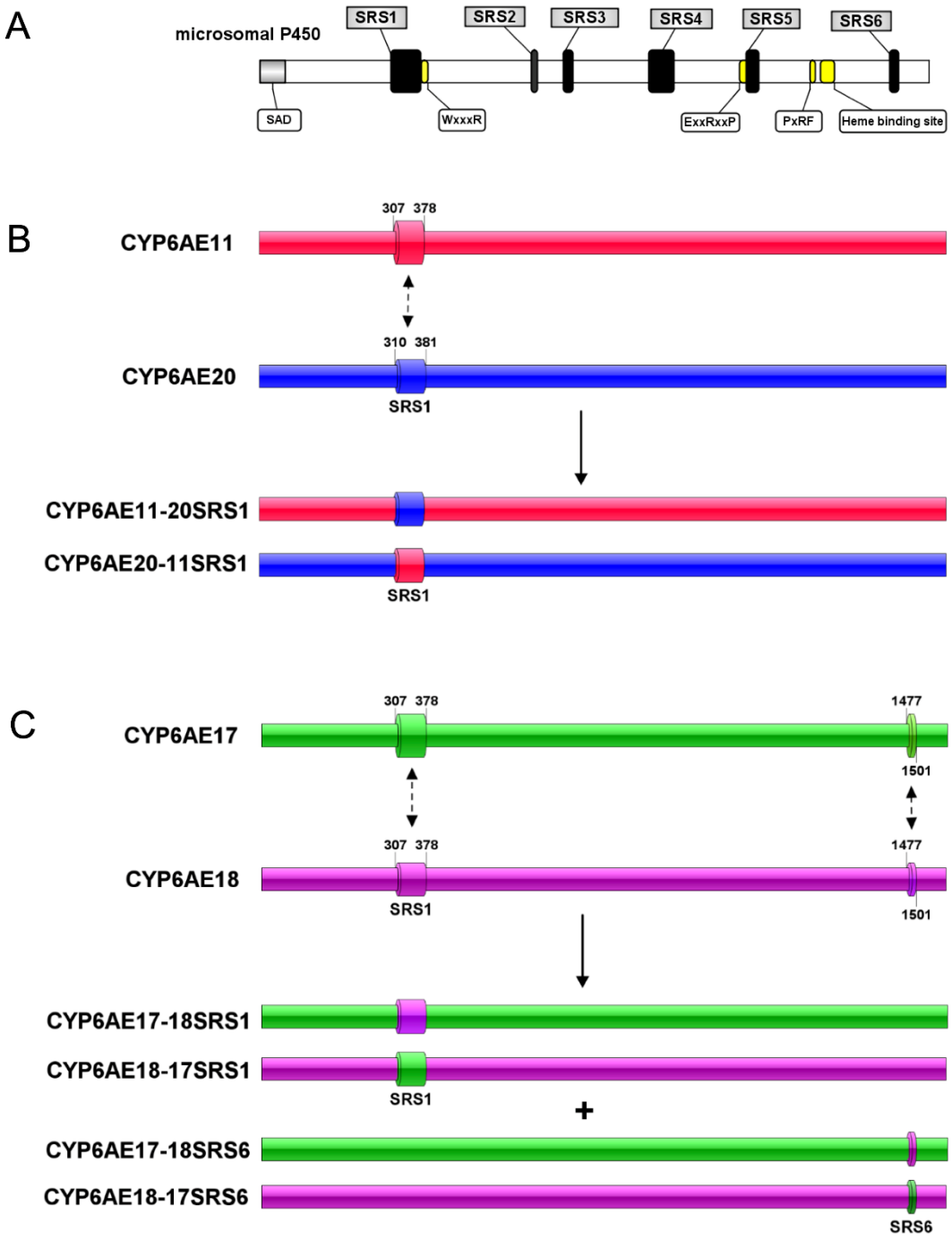

Figure 2. Construction of CYP6AE mutants. A: Typical structure of microsomal P450 protein, SRS, SAD (membrane-embedded signal anchor domain) and five conserved regions of microsomal P450 (WxxxR motif, A(A,G)x(E,Q)T motif, ExxRxxP motif, PxRF motif and Heme binding site) were marked. B: SRS1 exchanging of CYP6AE11/20; C: SRS1/SRS6 exchanging of CYP6AE17/18. Pictures were illustrated by IBS software (Liu et al., 2015).

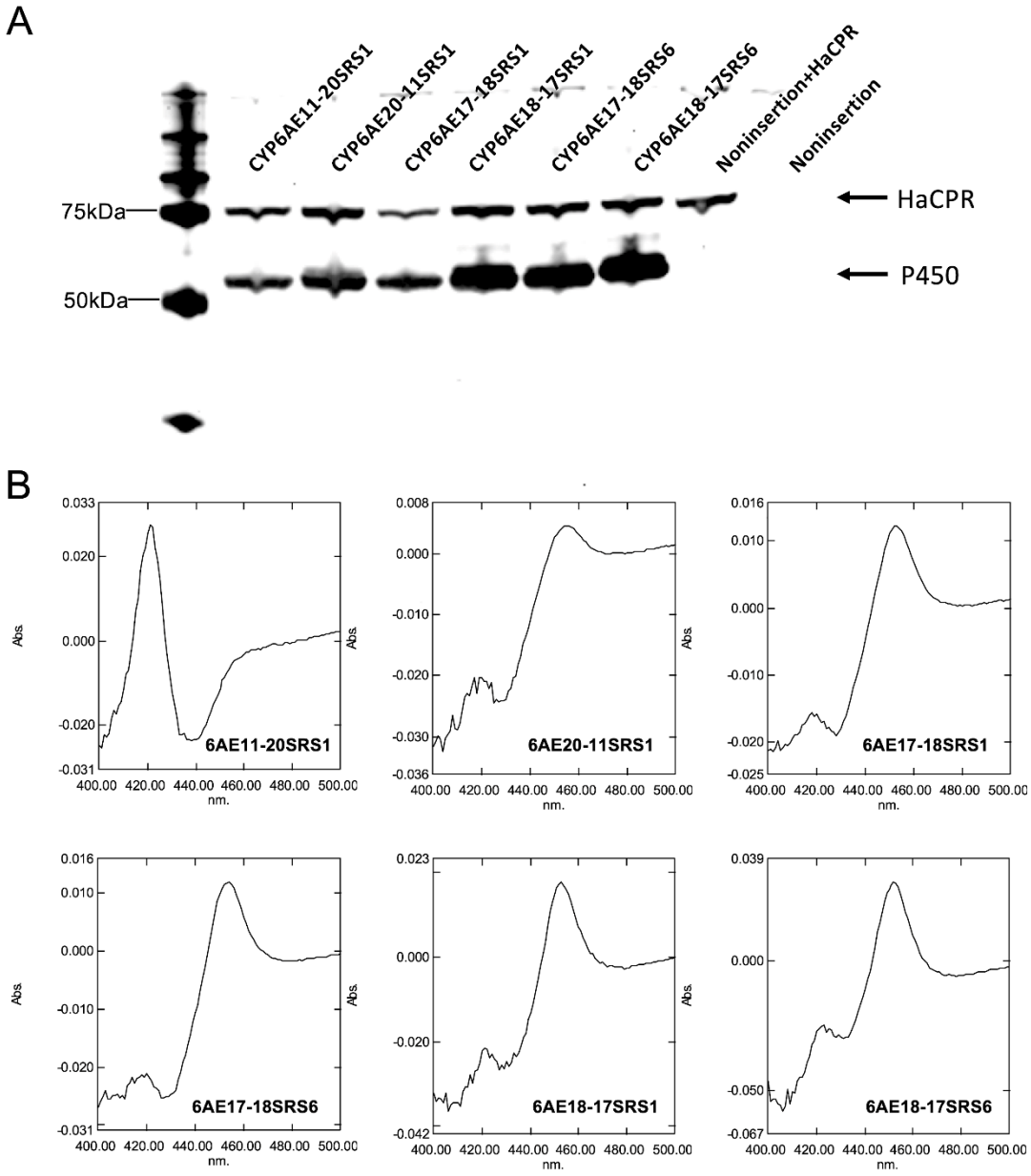

Figure 3. Identification of recombinant P450 mutants. A. Western Blot. 20μg purified microsomal protein with co-expressed P450 and HaCPR was loaded for each sample. B. Reduced CO-difference spectra of heterologously expressed CYP6AE hybrid mutants. Sf9 cells expressing individual P450 mutant were lysed and subjected to CO-difference spectral analysis.

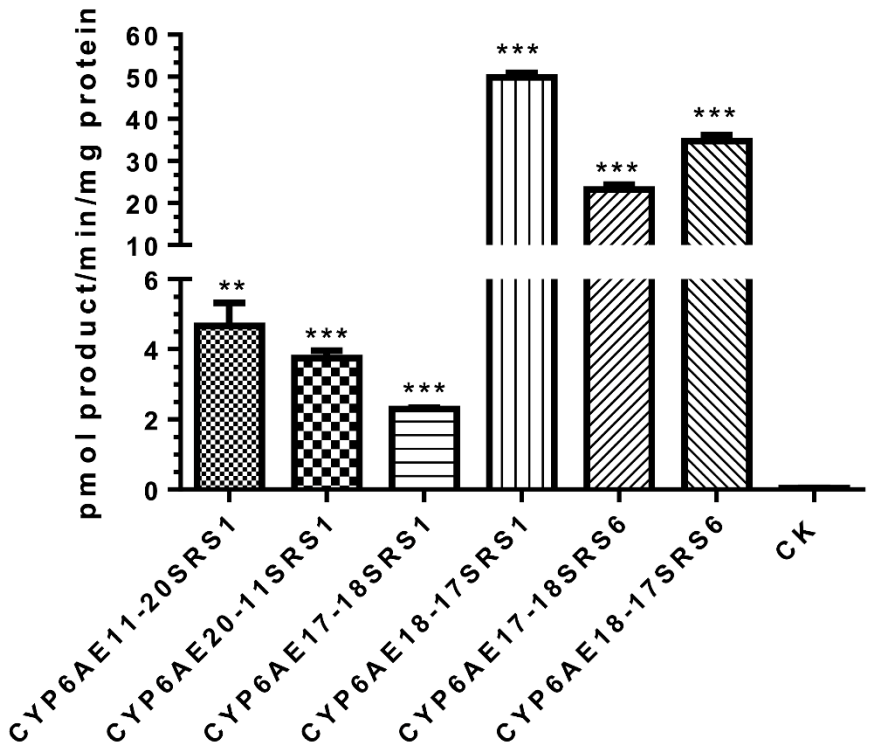

Figure 4. Qualitative enzyme activity tests toward esfenvalerate with six CYP6AE P450 mutants. ** means $p<0.01$ (t-test); *** means $p<0.001$ (t-test). CK means non-insertion control.

A

	SRS1																						SRS6							
							109			112							120	121						495	496					
6AE11	G	R	E	V	S	E	Y	V	D	K	E	R	F	T	Q	N	L	F	S	T	S	G	N	K	E	P	N	S	F	V	S	Q
6AE17	G	R	E	I	S	E	F	G	H	R	E	R	L	A	K	N	L	F	S	N	S	G	D	R	T	P	K	S	T	I	T	Q
6AE18	G	H	E	I	S	D	Y	A	H	R	E	R	M	S	K	N	L	F	A	T	H	G	D	R	S	A	K	T	I	V	T	Q
6AE20	G	R	E	S	S	D	Y	S	G	S	E	I	T	T	Q	N	V	F	F	N	A	G	D	R	D	A	R	T	F	L	T	Q

B

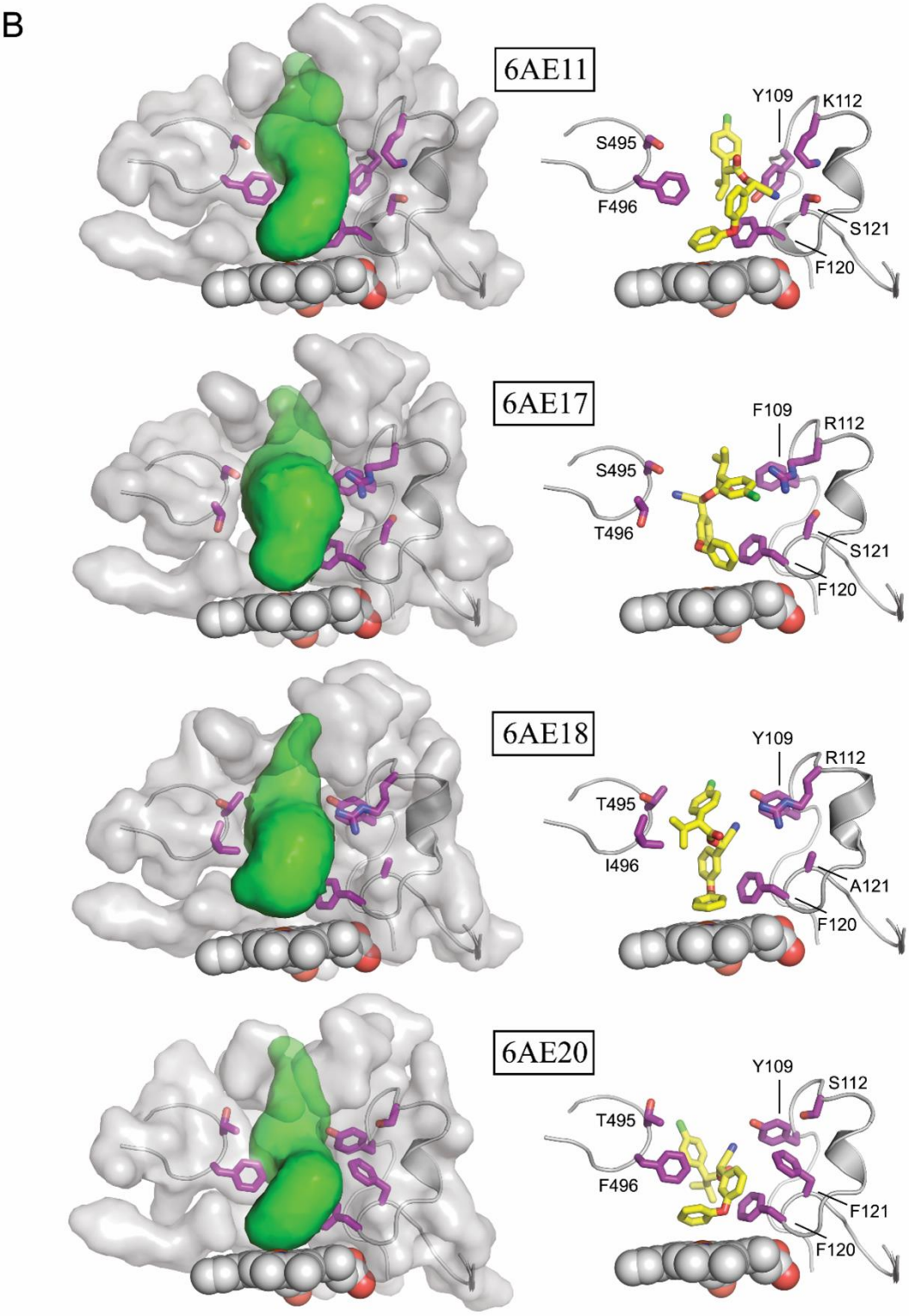

Figure 5. P450 homology models and docking predictions for esfenvalerate. **A:** sequence alignment of SRS1 and SRS6 sections. Residues highlighted in purple are predicted to line the active site of each enzyme (see B) and are numbered according to the 6AE11 sequence (GenBank: AEY75583.1). **B:** Left panels show the volume of each active site cavity depicted in green. The SRS1, 2, 3, 5 and 6 sections are shown in semi-transparent surface; SRS4 is not shown to aid visualisation. SRS1 and SRS6 sections are additionally shown as ribbon. SRS1 and SRS6 residues lining the cavity are in purple sticks. The heme group is in grey space-fill. Right panels show docked poses of esfenvalerate as yellow sticks. SRS1 and SRS6 residues lining the cavity are in purple sticks and numbered according to the 6AE11 sequence (see A).

Table 1

Kinetics of four *H. armigera* P450s and their hybrids in the metabolism of esfenvalerate

P450s	*V*max (pmol/min/pmol P450)	*K*m (μM)	Clint[a] *V*max/*K*m
CYP6AE11[b]	2.3±0.1	5.9±0.7	0.39
CYP6AE11-20SRS1	24.7±2.5[c]	6.6±1.7	-
CYP6AE20	n.d.[d]	n.d.	n.d.
CYP6AE20-11SRS1	0.17±0.001	3.7±0.6	0.05
CYP6AE17[b]	1.5±0.04	5.5±0.4	0.27
CYP6AE17-18SRS1	0.19±0.01	8.3±1.6	0.02
CYP6AE17-18SRS6	1.7±0.11	11.4±1.9	0.15
CYP6AE18[b]	0.1±0.01	2.8±0.5	0.04
CYP6AE18-17SRS1	1.5±0.1	6.0±1.2	0.25
CYP6AE18-17SRS6	0.72±0.05	1.8±0.5	0.4

[a] Intrinsic clearance.

[b] Data from Shi et al. (2018).

[c] pmol/min/mg protein.

[d] Not detected.